Journal of Elasticity
https://doi.org/10.1007/s10659-024-10055-y

RESEARCH

Modelling the Deformation of Polydomain Liquid Crystal Elastomers as a State of Hyperelasticity

Afshin Anssari-Benam[1] · Zhengxuan Wei[2] · Ruobing Bai[2]

Received: 30 January 2024 / Accepted: 13 February 2024

Abstract
A hyperelasticity modelling approach is employed for capturing various and complex mechanical behaviours exhibited by macroscopically isotropic polydomain liquid crystal elastomers (LCEs). These include the highly non-linear behaviour of nematic-genesis polydomain LCEs, and the soft elasticity plateau in isotropic-genesis polydomain LCEs, under finite multimodal deformations (uniaxial and pure shear) using in-house synthesised acrylate-based LCE samples. Examples of application to capturing continuous softening (i.e., in the primary loading path), discontinuous softening (i.e., in the unloading path) and auxetic behaviours are also demonstrated on using extant datasets. It is shown that our comparatively simple model, which breaks away from the neo-classical theory of liquid crystal elastomers, captures the foregoing behaviours favourably, simply as states of hyperelasticity. Improved modelling results obtained by our approach compared with the existing models are also discussed. Given the success of the considered model in application to these datasets and deformations, the simplicity of its functional form (and thereby its implementation), and comparatively low(er) number of parameters, the presented isotropic hyperelastic strain energy function here is suggested for: (i) modelling the general mechanical behaviour of LCEs, (ii) the backbone in the neo-classical theory, and/or (iii) the basic hyperelastic model in other frameworks where the incorporation of the director, anisotropy, viscoelasticity, temperature, softening etc parameters may be required.

Keywords Polydomain liquid crystal elastomers · Hyperelasticity · Finite elasticity · Soft elasticity · Constitutive modelling

Mathematics Subject Classification 74-10 · 74A20 · 74B20

1 Introduction

Liquid crystal elastomers (LCEs) are soft active materials made of liquid crystal molecules cross-linked with rubber-like polymer networks. In a typical LCE, the rod-like liquid crystal

✉ R. Bai
ru.bai@northeastern.edu

[1] Cardiovascular Engineering Research Lab (CERL), School of Mechanical and Design Engineering, University of Portsmouth, Anglesea Road, Portsmouth, PO1 3DJ, UK

[2] Department of Mechanical and Industrial Engineering, College of Engineering, Northeastern University, Boston, Massachusetts, 02115, USA

Published online: 26 February 2024

mesogens are linked with chains of a stretchable amorphous polymer network. At room temperatures, these mesogens form a *nematic* phase with an orientational order, but transform into an *isotropic* phase (i.e., no orientational order) above a nematic–isotropic transition temperature (e.g., around 60 °C) [1]. The low-temperature nematic phase can be either *monodomain* with a uniform mesogen orientation or *polydomain* with many coexisting domains of different mesogen orientations.

While the literature may sometimes broadly refer to these materials under the generic title of LCEs, it is important to distinguish the foregoing different phases and domain formations, as they portend significantly different mechanical behaviours and stress – deformation responses. Following Biggins et al. [2] and Wei et al. [3], we cast the following brief and precise categories of LCEs: (i) Isotropic-genesis polydomain LCEs, where an LCE sample is cross-linked in the isotropic phase of its mesogens; (ii) Nematic-genesis polydomain LCEs, where an LCE sample is cross-linked in the nematic phase of mesogens; and (iii) Nematic monodomain LCEs, where an LCE sample has a uniform mesogen alignment (i.e., director) throughout the entire material in the nematic phase of mesogens. We note similar classifications (with various categories) of LCEs in the works of Tokumoto et al. [4] and Lee and Bhattacharya [5]. The first two category of LCEs exhibit a macroscopically isotropic mechanical behaviour, while nematic monodomain LCEs have an anisotropic mechanical response due to the uniform mesogen order. The focus of the current work is on macroscopically isotropic polydomain LCEs, which at the ideal limit, are considered incompressible hyperelastic soft solids [4, 5].

The foregoing classes of polydomain LCEs evince interesting but complex mechanical behaviours. Of particular note, in addition to the highly non-linear stress–deformation response exhibited by both nematic- and isotropic-genesis polydomain LCEs, is a pronounced mode of ‘soft elasticity’ demonstrated by the latter type, characterised by a plateau in the uniaxial stress–stretch curves of these materials (e.g., see the experimental work of Urayama et al. [6] and the theoretical approach of Biggins et al. [7]). We note as well the recent works of Gleeson and co-workers that report on a ‘semi-soft’ behaviour in their acrylate-based monodomain LCE samples (e.g., [8, 9]), which at a macro stress–deformation level appears similar to that in the stress–strain curves of nematic-genesis polydomain LCEs. The soft elasticity plateau in strain–deformation curves is indicative of very low elastic energy, i.e., a small stress, required to induce large deformations, and is attributed to the director rotation from a randomly oriented to a uniformly aligned domain structure [6]. Other examples of the complex mechanical responses of LCEs include the auxetic behaviour by which the overall volume of the sample is preserved while the sample dimension in one direction (say thickness) increases with the increase in the applied deformation (see, e.g., [10]). Discontinuous softening, i.e., softening in the unloading path akin to the Mullins effect in rubber-like materials, is another feature in the mechanical behaviour of LCEs (see, e.g., [11]), which further exacerbates the complexity of modelling the holistic mechanical behaviour of these materials.

The prevailing modelling approach to the finite deformation of LCEs is perhaps the neo-classical theory [12–15]. The stored energy function in this framework, following the Gaussian molecular network assumption of rubber elasticity, is the neo-Hookean strain energy function, augmented by a ‘step-length’ tensor denoted by $\mathcal{L}$, and an ‘anisotropy parameter’ typically represented by r. Tensor $\mathcal{L}$ effectively describes the spontaneous deformation of the subject LCE via the anisotropy parameter r, which solely depends on the order parameter of the LC mesogens, i.e., the degree of directional alignment of these molecules along the director. While being the pioneering theory in modelling the soft elasticity phenomenon in LCEs and accounting for the rotation of director, the neo-classical modelling approach suffers from the following well-understood shortcomings.

First, as described by DeSimone and co-workers [16, 17], the neo-classical theory is not well-suited for capturing the behaviour of LCEs at larger deformations. This is due to the inherent limitation of the neo-Hookean model, which similar to its classical applications in rubber elasticity, cannot provide a good fit to the data at larger levels of deformation. We note the attempts for considering other strain energies within the neo-classical framework such as Mooney-Rivlin [5] and Ogden-type [17] models etc. However, the former model too has well-documented shortcomings in capturing various behaviours of rubber-like materials, while the latter model has been shown susceptible to ill-posed effects when applied to soft(er) solids [18–20]. Therefore, a strain energy function with a more comprehensive functional form that can better capture the deformation of LCE specimens across their full-range of deformation, and remain free from ill-posed modelling results, would be more desirable.

Second, the application of the neo-classical theory (irrespective of the choice of the embedded strain energy) has mostly been limited to a single mode of deformation, most often uniaxial deformation. The capability of this theory for simultaneous modelling of various deformation modes therefore remains largely unexplored. A notable and rare study where uniaxial, pure shear and biaxial deformations of polydomain LCEs are considered is that of Tokumoto et al. [4], in which, interestingly, a more complex model had to be presented.

Third, even within uniaxial deformation, the neo-classical theory postulates a threshold stretch, almost as a switch, below which the theory emulates the occurrence of soft elasticity. However, in addition to the difficulty of measuring an exact value for this threshold stretch experimentally, mathematical/computational implementation of such models will entail non-smoothness at the point of transition (i.e., threshold deformation). It is more advantageous to have a model that captures soft elasticity and the proceeding rubber-like behaviour with a continuous function.

Fourth, augmentation of the basic hyperelastic function to include an 'anisotropy parameter' r for application to macroscopically isotropic nematic- and isotropic-genesis polydomain LCEs would seem unnecessary. Similarly, incorporating a 'step-length' tensor $\mathcal{L}$ for capturing soft elasticity, where it has been shown that the postulated director rotations are not necessary for this phenomenon (see, e.g., the work of Fried and Sellers [21]), appears superfluous. It would therefore seem more appropriate to work with a model that captures the mechanical behaviours of interest in LCEs without the unnecessary additions that are brought about by the neo-classical theory.

Fifth, and finally, if other mechanical features of LCEs such as discontinuous softening (in the unloading path) and auxetic behaviours etc are also to be considered, the neo-classical theory with the aforementioned extra parameters already added to the basic strain energy function makes it more difficult to incorporate further/additional variables and identify meaningful parameter values through a process of fitting and minimisation. We note here recent alternative models by Mihai and co-workers on using modified neo-Hookean and Ogden models [22, 23]. However, those modelling approaches still incorporate elaborate mathematical models with a relatively high number of terms and parameters, including auxiliary functions, which in an attempt to keep them as simple as possible "*their approximation of the observed phenomena are not the best*" [23]. In this spirit, a simpler modelling approach that is more amenable to capturing these behaviours with a more reduced set of model parameters/variables may prove more practical.

In an attempt towards alleviating these five shortcomings recounted in the foregoing, here we wish to put forward a simple isotropic incompressible hyperelastic strain energy function for application to the finite deformation of nematic- and isotropic-genesis polydomain LCEs. To this end, we undertake to model the uniaxial and pure shear deformations of our in-house synthesised acrylate-based LCEs, simply as states of hyperelasticity, without incorporating the concept of director rotation and/or step-length parameters etc. The model is simultaneously fitted to the datasets, and is shown to favourably capture the highly nonlinear deformation and soft elasticity modes exhibited by the samples. To further showcase the capability of the model, we also present its application to capturing continuous softening (in the primary loading path), discontinuous softening (in unloading path) and the auxetic behaviour of LCE samples using extant experimental data. By considering this wide range of datasets and behaviours, our intention is to demonstrate the capability and merit of our model over the currently existing neo-Hookean, Mooney-Rivlin, and Ogden type models, for capturing the mechanical behaviour of LCEs. For applications where the use of neo-classical theory and/or incorporation of anisotropy, temperature, and rate-effects is necessary, the presented model here may serve as a hyperelastic backbone in the required augmented modelling frameworks and theories.

In §2 a brief summary of the hyperelastic strain energy function of interest will be presented. The experimental methodology, including sample synthesis and preparation, as well as the mechanical testing setup will be described in §3. The application of the model to experimental data will be demonstrated in §4. Accordingly, the model is fitted simultaneously to uniaxial and pure shear datasets of our in-house synthesised nematic- and isotropic-genesis polydomain LCE specimens. In addition, we will also consider the application of the model to capturing the continuous softening, i.e., the gradual softening in the primary loading path which eventually leads to failure, of the explicit type discussed in [24], in a nematic LCE sample under uniaxial deforamtion due to He et al. [25]. Next, discontinuous softening behaviour (in the unloading path) of a nematic-genesis polydomain LCE originally due to Merkel et al. [11], also exhibiting a permanent set in the load-free configuration, will be modelled. For this purpose, we will employ the recently proposed extension to the classical pseudo-elasticity theory of Ogden and Roxburgh [26], by Anssari-Benam et al. [27]. Finally in this section we will consider the application of the model to the uniaxial deformation of a monodomain LCE sample reported in Raistrick et al. [10], exhibiting an auxetic behaviour. The hyperelastic model will be directly applied to this dataset, without any additional complexities that arise from considering director order tensors and/or Landau-de Gennes expansions etc considered in previous studies to capture such auxetic behaviours (e.g., in [23]). The improved modelling results will be presented and highlighted. Concluding remarks will be conferred in §5. Given these promising early modelling results provided by the considered strain energy function here, the application of this hyperelastic function to modelling the general mechanical behaviour of LCEs either as a stand-alone model or as the backbone in the neo-classical theory, or indeed as the basic hyperelastic model in other augmented frameworks and theories, is proposed.

2 The Hyperelastic Strain Energy Function

The hyperelastic model of interest here is of binomial form; i.e., $W(I_1, I_2) = f(I_1) + g(I_2)$, first introduced in [28], as the following function:

$$\begin{aligned} W(I_1, I_2) = {} & \sum_{j=1} \frac{3(n_j - 1)}{2n_j} \mu_j N_j \left[\frac{1}{3N_j (n_j - 1)} (I_1 - 3)^{\beta_j} - \ln\left(\frac{I_1 - 3N_j}{3 - 3N_j} \right)^{\beta_j} \right] \\ & + \sum_{k=1} C_k \left[\left(\frac{I_2}{3} \right)^{\epsilon_k} - 1 \right], \end{aligned} \tag{1}$$

where:

$$\begin{cases} n_j, \mu_j, N_j, C_k \in \mathbb{R}^+, \\ \beta_j, \epsilon_k \in \mathbb{R}, \end{cases} \tag{2}$$

are model parameters, and I_1 and I_2 are the first and second principal invariants of $\mathbf{B}(= \mathbf{F}\mathbf{F}^{\mathrm{T}})$, respectively. The infinitesimal shear modulus μ_0 for this model is:

$$\mu_0 = \sum_{j=1} \frac{\mu_j \beta_j N_j \left(1 - n_j\right)}{n_j \left(1 - N_j\right)} + \sum_{k=1} \frac{2\epsilon_k}{3} C_k. \tag{3}$$

The generalised neo-Hookean part of the model; i.e.,

$$f\left(I_1\right) = \sum_{j=1} \frac{3\left(n_j - 1\right)}{2n_j} \mu_j N_j \left[\frac{1}{3N_j\left(n_j - 1\right)} \left(I_1 - 3\right)^{\beta_j} - \ln\left(\frac{I_1 - 3N_j}{3 - 3N_j}\right)^{\beta_j} \right], \tag{4}$$

is a generalisation obtained from the response function first introduced in [29], from a rational approximant in I_1 of [1/1] order to a [β/1] order (see [28]). The I_2-term; i.e.,

$$g\left(I_2\right) = \sum_{k=1} C_k \left[\left(\frac{I_2}{3}\right)^{\epsilon_k} - 1 \right], \tag{5}$$

is a generalisation of the basic $\sqrt{I_2}$ function presented by Carroll [30].

Remark 1 In the original presentation [28], it was stipulated that N has to be single valued; i.e., cannot be subscripted, unlike the other model parameters. However, we note here, when using the multi-term expansion of the model, that in any case the value of the limiting extensibility will be *a priori* determined by the minimum value of N_j. Therefore, there is no need for the overtly prescriptive restriction in [28], to limit N to only a single value. This notion is further underlined in cases where $N < 1$, which implies no limiting extensibility in the first place. This nuance distinction is made here with respect to the original presentation in [28].

Remark 2 The conditions in Eq. (2) are those originally proposed in [28]. For the empirical relationship $W_2 \geq 0$ to hold true, one would require $C_k \geq 0$ and $\epsilon_k \geq 0$, or alternatively $C_k \leq 0$ and $\epsilon_k \leq 0$. However, as also considered by Mihai and Goriely [31], the prediction of some mechanical behaviours such as the *reverse* Poynting effect will lead to the violation of that empirical inequality. As such, the condition in Eq. $(2)_2$ was considered instead in [28] for ϵ_k. In the same spirit, the restriction on C_k may also be relaxed to $C_k \in \mathbb{R}$. In particular, note that when both $C_k \leq 0$ and $\epsilon_k \leq 0$, the empirical relationship $W_2 \geq 0$ remains intact.

The favourable application of this model to a wide range of soft materials including natural unfilled and filled rubbers, hydrogels, and biomaterials under various deformation modes was demonstrated in [28]. In addition, it is noteworthy that the generalised neo-Hookean part of the model $f\left(I_1\right)$ is *parent* to many of the existing models in the literature, from the neo-Hookean [32] to limiting chain extensibility model of Gent [33], and those of

Anssari-Benam and Horgan [34] and Anssari-Benam and Bucchi [35, 36]; *vide infra*. It can be verified that using the one-term expansion with $\beta = 1$, we have, respectively,

$$\begin{cases} \lim\limits_{N\to\infty} f\left(I_1\right) = \lim\limits_{n\to 1} f\left(I_1\right) = \dfrac{1}{2}\mu\left(I_1 - 3\right), \\ \lim\limits_{n\to\infty} f\left(I_1\right) = -\dfrac{3}{2}\mu_0\left(N-1\right)\ln\left(-\dfrac{I_1 - 3N}{3N-3}\right) = -\dfrac{1}{2}J_m\,\mu_0\ln\left(1 - \dfrac{I_1 - 3}{J_m}\right), \\ f\left(I_1\right) = \dfrac{3\left(n-1\right)}{2n}\mu N\left[\dfrac{1}{3N\left(n-1\right)}\left(I_1 - 3\right) - \ln\left(\dfrac{I_1 - 3N}{3-3N}\right)\right], \\ f\left(I_1\right) \overset{n=3}{=\!=} \mu N\left[\dfrac{1}{6N}\left(I_1 - 3\right) - \ln\left(\dfrac{I_1 - 3N}{3-3N}\right)\right]. \end{cases} \tag{6}$$

Therefore, the model in Eq. (1) appears to be a broad representation of the mechanical behaviour of isotropic incompressible soft materials, and of hyperelastic models.

3 Samples Preparation and Experiments

For the purpose of synthesising our in-house specimens, 4-Bis-[4-(3-acryloyloxypropypropyloxy) benzoyloxy]-2-methylbenzene (RM257, LC mesogen) was acquired from Daken Chemical, and Pentaerythritol tetra(3-mercaptopropionate) (PETMP, crosslinker), 2,2-(ethylenedioxy)diethane-thiol (EDDET, spacer), 2,6-di-tert-butyl-4-methylphenol (BHT, antioxidant), dipropylamine (DPA, catalyst), and toluene (solvent) were purchased from Sigma-Aldrich. All materials were used in their as-received condition without further purification.

3.1 Synthesis of Isotropic- and Nematic-Genesis Liquid Crystal Elastomers

All our LCE samples were synthesised following the well-established thiol-acrylate Michael addition reaction described in [37, 38]. To synthesise an isotropic-genesis LCE, 8 g of RM257, 0.16 g of BHT, and 3.2 g of toluene (40 wt% of RM257) were mixed and heated to 85 °C to form a homogeneous solution. The solution was cooled to room temperature, and 0.434 g of PETMP and 1.83 g of EDDET were subsequently added. The solution was then mixed and vacuumed by a FlackTek SpeedMixer for 1.5 minutes to reach homogeneity. Finally, a separate solution of catalyst of 1.136 g (with a weight ratio of DPA and toluene at 1:50) was added, and the solution was mixed and vacuumed for another 1.5 minutes to reach homogeneity. The final solution was poured into acrylic molds of 5×1×0.1 cm^3 or 14×10×0.1 cm^3 for complete polymerization. After 12 hours, the samples were taken out from the mould and placed into a vacuum oven at 80 °C and 508 mmHg for 24 hours to evaporate the toluene. During the polymerization, BHT absorbs the extra free radicals in the mixture. This, together with the solvent toluene, yields an isotropic-genesis LCE [38]. To synthesise a nematic-genesis LCE, the same process was followed but without the addition of BHT in the solution.

3.2 Uniaxial and Pure Shear Tests

Uniaxial and pure shear tests were conducted on the synthesised LCE samples using an Instron tensile tester (Instron 34TM-5). For uniaxial tensile tests (Fig. 1a), samples of 0.09-0.12 cm thickness were cut into long rectangular strips of 0.8 cm width and mounted into

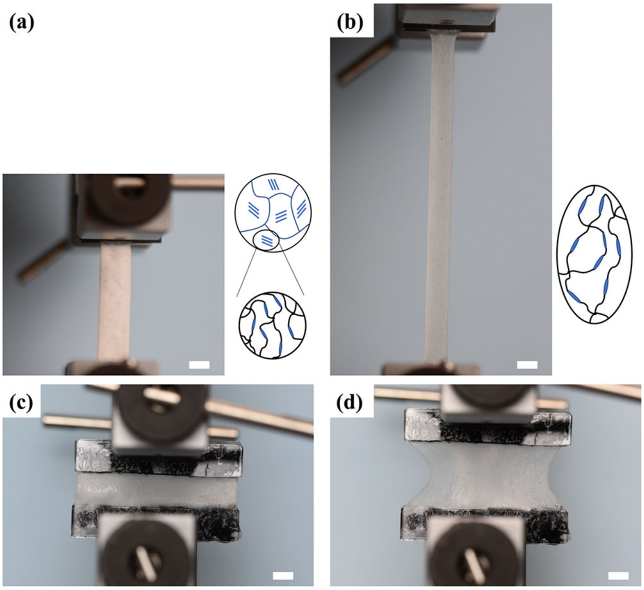

Fig. 1 Uniaxial tensile and pure shear deformation test of the in-house nematic-genesis polydomain LCE specimens: (a) reference and (b) deformed states of a uniaxial sample; (c) reference and (d) deformed states of a pure shear sample. The inset schematics illustrate the molecular structures of the polydomain LCE before and after the deformation. The scale bar represents 1 cm in all figures

the tensile tester to form a gauge length of 4.5 cm. For pure shear tests (Fig. 1c), samples of the same thickness range were cut into wide rectangular sheets of 5 cm width, glued to two pairs of acrylic grips, and mounted into the tensile tester to form a gauge length of 1 cm. The samples were then stretched by the tensile tester (e.g., Figs. 1b and 1c for uniaxial and pure shear deformations, respectively) until catastrophic fracture at room temperature of 20-22 °C, with the force and displacement recorded by the machine. Both experiments were performed under quasi-static conditions, with the deformation rate set at 0.01 s^{-1}.

4 Modelling Results

In this section we proceed with applying the model in Eq. (1) to a wide range of experimental data and deformations. The considered datasets encompass multimodal deformations (i.e., uniaxial and pure shear) of our in-house nematic- and isotropic-genesis polydomain LCE specimens, and extant datasets including continuous softening (in the primary loading path) of a nematic LCE sample under uniaxial loading, discontinuous softening behaviour (in the unloading path) under uniaxial deformation of a nematic-genesis polydomain LCE also exhibiting permanent set, and uniaxial deformation of a monodomain LCE sample with auxetic behaviour.

For each deformation, we derive and present the related (engineering) stress – deformation relationships and fit those relationships to the data, by minimising the residual sum of squares (RSS) function defined as: $\text{RSS} = \sum_i \left(P^{model} - P^{experiment}\right)_i^2$, where i is the number of data points and P is the engineering stress (or alternatively T as the Cauchy stress, depending on the source data). The minimisation is performed via an in-house developed code in MATLAB®, using the genetic algorithm (GA) function. The coefficient of determination R^2 values are reported as a measure of the goodness of the obtained fits.

4.1 Uniaxial and Pure Shear Deformations

We start by modelling the multimodal (uniaxial and pure shear) deformations of our nematic- and isotropic-genesis polydomain LCE samples. For doing so, we first derive and present the (engineering) stress – stretch (λ) relationships. Accordingly, we employ the representation formula for the Cauchy stress as:

$$\mathbf{T} = -p\,\mathbf{I} + 2W_1\,\mathbf{B} - 2W_2\mathbf{B}^{-1}\,, \tag{7}$$

where $\mathbf{B}$ is the left Cauchy-Green deformation tensor and $\mathbf{B}^{-1}$ is its inverse, p is the arbitrary Lagrange multiplier enforcing the condition of incompressibility, and $\mathbf{I}$ is the identity tensor. Note that W_1 and W_2 are the partial derivatives of the strain energy function W in Eq. (1) with respect to I_1 and I_2, where $I_1 = \lambda_1^2 + \lambda_2^2 + \lambda_3^3$ and $I_2 = \lambda_1^{-2} + \lambda_2^{-2} + \lambda_3^{-2}$ are the first and second principal invariants of $\mathbf{B}$, respectively, and $I_3 = 1$ due to incompressibility.

In uniaxial deformation we have $\lambda_1 = \lambda$ and $\lambda_2 = \lambda_3 = \lambda^{-0.5}$. Subject to the assumption of plane stress ($T_{33} = 0$), we find from Eqs. (1) and (7):

$$\begin{aligned} T_{uni} = {} & \sum_{j=1} \frac{\mu_j \beta_j}{n_j} \frac{I_1 (I_1 - 3)^{\beta_j - 1} + 3N_j \left[1 - (I_1 - 3)^{\beta_j - 1}\right] - 3n_j N_j}{I_1 - 3N_j} \left(\lambda^2 - \frac{1}{\lambda}\right) \\ & + \sum_{k=1} \frac{2C_k \epsilon_k}{3^{\epsilon_k}} I_2^{\epsilon_k - 1} \left(\lambda - \frac{1}{\lambda^2}\right). \end{aligned} \tag{8}$$

The resultant engineering stress $\mathbf{P}$ components may be obtained from $\mathbf{T}$ on using $\mathbf{T} = \mathbf{F}\,\mathbf{P}$, where $\mathbf{F}$ is the deformation gradient tensor. It follows:

$$\begin{aligned} P_{uni} = {} & \sum_{j=1} \frac{\mu_j \beta_j}{n_j} \frac{I_1 (I_1 - 3)^{\beta_j - 1} + 3N_j \left[1 - (I_1 - 3)^{\beta_j - 1}\right] - 3n_j N_j}{I_1 - 3N_j} \left(\lambda - \frac{1}{\lambda^2}\right) \\ & + \sum_{k=1} \frac{2C_k \epsilon_k}{3^{\epsilon_k}} I_2^{\epsilon_k - 1} \left(1 - \frac{1}{\lambda^3}\right). \end{aligned} \tag{9}$$

Note that here $I_1 = \lambda^2 + 2\lambda^{-1}$ and $I_2 = 2\lambda + \lambda^{-2}$.

Similarly, for pure shear deformation we have that $\lambda_1 = \lambda$, $\lambda_2 = 1$ and $\lambda_3 = \lambda^{-1}$, which yields:

$$\begin{aligned} T_{ps} = {} & \left\{ \sum_{j=1} \frac{\mu_j \beta_j}{n_j} \frac{I_1 (I_1 - 3)^{\beta_j - 1} + 3N_j \left[1 - (I_1 - 3)^{\beta_j - 1}\right] - 3n_j N_j}{I_1 - 3N_j} \right. \\ & \left. + \sum_{k=1} \frac{2C_k \epsilon_k}{3^{\epsilon_k}} I_2^{\epsilon_k - 1} \right\} \left(\lambda^2 - \frac{1}{\lambda^2}\right), \end{aligned} \tag{10}$$

Table 1 Obtained model parameter values identified by fitting the one-term expansion of the model to the mutimodal deformation data of our nematic-genesis polydomain LCE specimen. Note that $R^2_{uni} = 0.99_8$ and $R^2_{ps} = 0.99_4$, for uniaxial and pure shear deformations, respectively

μ [MPa]	N [-]	n [-]	β [-]	C_2 [MPa]	ϵ [-]
0.02	0.96_5	0.85	2.39	2.87	0.28

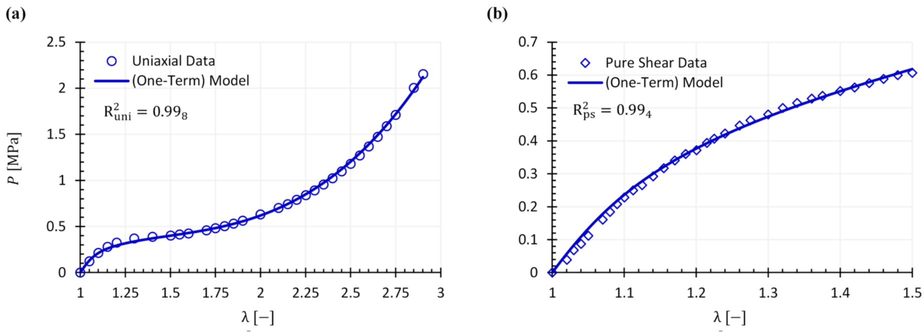

Fig. 2 Modelling results for the multimodal deformation dataset of our in-house nematic-genesis polydomain LCE specimens using the one-term expansion of the model in Eq. (1): (a) uniaxial; and (b) pure shear deformations

or, equivalently:

$$P_{ps} = \left\{ \sum_{j=1} \frac{\mu_j \beta_j}{n_j} \frac{I_1 (I_1 - 3)^{\beta_j - 1} + 3N_j \left[1 - (I_1 - 3)^{\beta_j - 1}\right] - 3n_j N_j}{I_1 - 3N_j} \right.$$
$$\left. + \sum_{k=1} \frac{2C_k \epsilon_k}{3^{\epsilon_k}} I_2^{\epsilon_k - 1} \right\} \left(\lambda - \frac{1}{\lambda^3} \right), \quad (11)$$

with $I_1 = I_2 = \lambda^2 + 1 + \lambda^{-2}$.

Equations (9) and (11) are subsequently fitted, simultaneously, to the datasets obtained under uniaxial and pure shear deformations, using the procedure described earlier in the prelude to this section. In the sequel we present the modelling results.

For the nematic-genesis polydomain LCE samples, we employ the one-term expansion of the model; i.e., $j = k = 1$, and fit the ensuing $P_{uni} - \lambda$ and $P_{ps} - \lambda$ relationships simultaneously to the data. The plots in Fig. 2 present the modelling results for a typical specimen, and Table 1 summarises the identified model parameter values. The tabulated numerical datapoints of this dataset have been presented in Appendix A, Table 7. It is observed that the one-term expansion of the model captures the multimodal deformations favourably, with R^2 values in excess of 0.99. For the interested reader, another modelling example from this batch of samples has been presented in Appendix B, Fig. 8.

For the isotropic-genesis polydomain LCE specimens, we utilise the two-term expansion of the model; i.e., $j = k = 2$, as it was empirically observed that the two-term expansion was the minimal expansion required to obtain favourable fits. The ensuing (engineering) stress – stretch relationships for uniaxial and pure shear deformations were simultaneously

Table 2 The identified model parameter values for our isotropic-genesis polydomain sample on using the two-term expansion of the model. Note that $R^2_{uni} = 0.99_6$ and $R^2_{ps} = 0.99_5$, for uniaxial and pure shear deformations, respectively

μ_1 [MPa]	N_1 [-]	n_1 [-]	β_1 [-]	C_1 [MPa]	ϵ_1 [-]
2.77×10^{-6}	0.76	0.99	3.52	-7.29	-0.14
μ_2 [MPa]	N_2 [-]	n_2 [-]	β_2 [-]	C_2 [MPa]	ϵ_2 [-]
0.00_4	0.82	0.14	1.00	3.94	-0.28_5

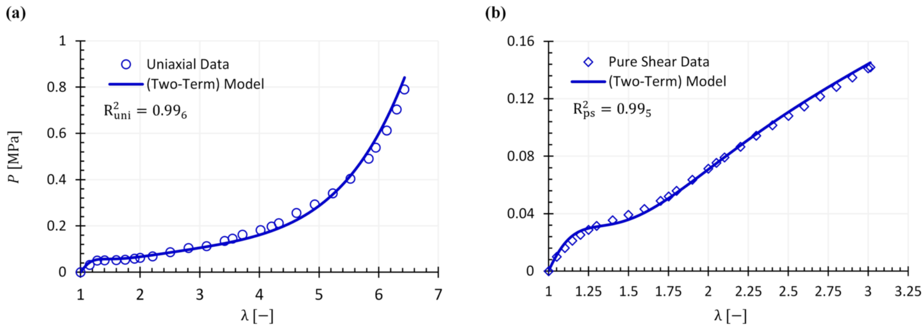

Fig. 3 Modelling results for the multimodal deformation dataset of our in-house isotropic-genesis polydomain LCE specimens using the two-term expansion of the model in Eq. (1): (a) uniaxial; and (b) pure shear deformations

fitted to the data. The fitting results for a typical specimen are presented in Fig. 3. The obtained model parameter values are given in Table 2. The tabulated numerical datapoints pertaining to this dataset have been provided in Table 8 of Appendix A. The performance of the two-term model appears exemplary, with R^2 values in excess of 0.99. The model captures the challenging behaviour of soft elasticity favourably, as purely a state of hyperelasticity without the need for incorporation of the so-called 'step-length' tensor or the 'anisotropy parameter'. For the interested reader, another modelling example from our pool of samples has been presented in Appendix B, Fig. 9.

It may be informative at this juncture to also consider the uniaxial and pure shear deformations of the isotropic-genesis polydomain specimens due to Tokumoto et al. [4]. The multiaxial mechanical behaviour of those specimens proved very complex, and an elaborate modelling scheme was proposed therein to capture those intricate behaviours [4]. Indeed, we observed that a three-term expansion of the model in Eq. (1) was required; i.e., $j = k = 3$, to properly capture the reported uniaxial and pure shear deformations of the specimens. Upon simultaneously fitting the ensuing $T_{uni} - \lambda$ and $T_{ps} - \lambda$ relationships to the data, the plots in Fig. 4 illustrate the modelling results. The identified model parameter values have been listed in Table 3. The tabulated numerical datapoints collated from [4] are given in Appendix A, Table 9. Not only the model is seen to capture well the soft elasticity mode in the uniaxial deformation, but also the challenging behaviour in pure shear is modelled favourably too. The R^2 values for the fits are in excess of 0.99.

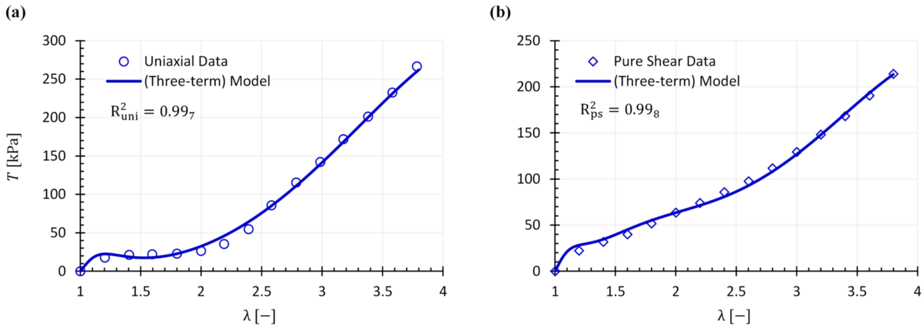

Fig. 4 Modelling results for the isotropic-genesis polydomain specimens due to Tokumoto et al. [4], using the three-term expansion: (a) uniaxial; and (b) pure shear deformations. Note that the stresses here are the Cauchy (T) stress

Table 3 Model parameter values for the isotropic-genesis polydomain specimens due to Tokumoto et al. [4], using the three-term expansion. Note that $R^2_{uni} = 0.99_7$ and $R^2_{ps} = 0.99_8$, for uniaxial and pure shear deformations, respectively

μ_1 [kPa]	N_1 [-]	n_1 [-]	β_1 [-]	C_1 [kPa]	ϵ_1 [-]
19.54	0.95	0.84	1.39	500.00	-0.24
μ_2 [kPa]	N_2 [-]	n_2 [-]	β_2 [-]	C_2 [kPa]	ϵ_2 [-]
-6.78	0.50	0.17	1.14	205.25	-1.85
μ_3 [kPa]	N_3 [-]	n_3 [-]	β_3 [-]	C_3 [kPa]	ϵ_3 [-]
12.77	27.31	0.09	1.04	-499.98	-1.14

4.2 Continuous Softening Under Uniaxial Loading in the Primary Loading Path

Modelling the continuous softening observed in the loading paths of soft solids (up to the onset of failure) using only a hyperelastic model, and hyperelastic constitutive parameters, was recently devised and discussed in [24]. We employ the same concept here to capture the softening behaviour observed in the uniaxial deformation of nematic LCE specimens of He et al. [25]. This dataset, in addition to the foregoing softening behaviour, also exhibits a soft elasticity mode that is distinct from those considered in the previous section, in that the soft elasticity behaviour here occurs right from the beginning of the deformation, as opposed to an initial hardening phase observed previously in the plots of Figs. 2 to 4. This experimental data is illustrated in Fig. 5. For modelling this behaviour, we employ the two-term expansion of the model in Eq. (1), and fit the ensuing $P_{uni} - \lambda$ relationship (Eq. (9)) to this dataset. The tabulated numerical datapoints associated with this set are provided in Table 10 of Appendix A. The results in Fig. 5 indicate a close correlation between the model and the data, with favourable predictions of both the soft elasticity phase and the softening behaviour. The value of R^2 for this fit is in excess of 0.99. The obtained model parameter values have been presented in Table 4. For the interested reader, the fitting results on using the one-term expansion of the model have also been presented in Fig. 10 of Appendix B. While the one-term expansion form still provides a good fit to the data, the judicious choice of the two-term expansion as the preferred option is clear by comparing the two fits.

Fig. 5 Modelling results for the nematic LCE specimens of He et al. [25] under uniaxial deformation on using the two-term expansion of the model

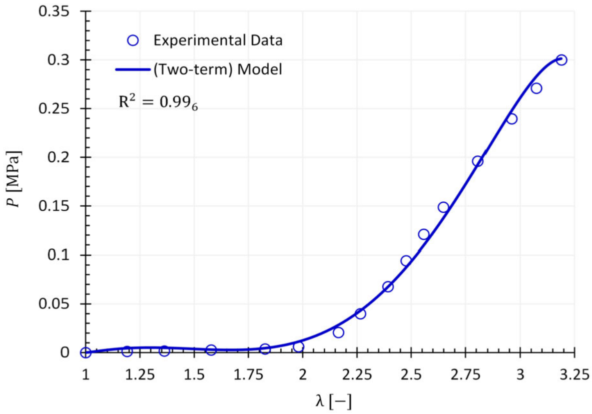

Table 4 Model parameter values for the nematic LCE specimens of He et al. [25] using the two-term expansion of the model. Note that $R^2 = 0.99_6$

μ_1 [MPa]	N_1 [-]	n_1 [-]	β_1 [-]	C_1 [MPa]	ϵ_1 [-]
0.06	6.19_5	0.17	1.00	1.46	0.008
μ_2 [MPa]	N_2 [-]	n_2 [-]	β_2 [-]	C_2 [MPa]	ϵ_2 [-]
0.007	4.05	0.92	2.61	0.15	0.06

4.3 Loading/Unloading, Discontinuous Softening and Permanent Set

The softening observed in the mechanical behaviour of rubber-like materials, and in particular filled rubbers, in the unloading path is generally known as the Mullins effect and is a well-studied phenomenon. The seminal theory of pseudo-elasticity by Ogden and Roxburgh [26] provides a versatile framework for modelling this behaviour in rubbers. Here we refer to this softening phenomenon as 'discontinuous' softening, to distinguish between this behaviour and the continuous and progressive softening in the primary loading path of the type discussed in [24], considered in the previous section.

In a recent study, Merkel et al. [11] demonstrated such discontinuous softening behaviour in nematic-genesis polydomain LCEs too, investigated under uniaxial loading and unloading at various temperatures. It was demonstrated that the samples, in addition to softening in the unloading path, also exhibit permanent set; i.e., a residual strain upon returning to the stress-free state. While the shape of the curves and the amount of the permanent set varied with temperature [11], Mihai and Goriely [22] developed a novel 'pseudo-anelastic' model to capture the temperature-independent behaviour based on the classical pseudo-elasticity theory devised by Dorfmann and Ogden [39] which also accounts for the permanent set. The model was then successfully applied to each stress – deformation curves of Merkel et al. [11], separately at each temperature [22].

The model by Mihai and Goriely [22], however, was developed within the neo-classical theory of LCEs, and as such accommodated the usual concepts of 'step-length' tensor and the 'anisotropy parameter'. In addition, it was deemed necessary to consider a four-term Ogden model for the basic hyperelastic function, and to account for the permanent set based on the theory of Dorfmann and Ogden [39] an additional 'auxiliary' function was also required

[22]. To incorporate the softening in the unloading path, of course, a damage parameter and function had to be considered as well. The combination of these add-ons renders the developed model rather intricate.

Here, to model the aforementioned discontinuous softening and permanent set at each temperature, we use the (one-term) hyperelastic model of Eq. (1), within the extended pseudo-elasticity framework recently developed by Anssari-Benam et al. [27], which captures both the softening and permanent set phenomena without the need for an auxiliary function etc. This, in combination with the lack of need to incorporate the 'step-length' tensor and the 'anisotropy parameter', results in a much simpler model to capture the Mullins effect in LCEs, and as will be shown in the sequel, with a favourable modelling outcome.

First, however, we present the theoretical underpinnings of the pseudo-elastic model. We briefly recall from [27] that the components of the Cauchy stress (T) are derived from a pseudo strain energy function $\widetilde{W}$ as:

$$T_i = \Omega\Gamma_i \frac{\partial \widetilde{W}}{\partial \Gamma_i} - p\,, \quad i = 1, 2, 3, \tag{12}$$

where:

$$\widetilde{W} \equiv W\left(\lambda_i, \Omega_i\right)\,, \quad i = 1, 2, 3, \tag{13}$$

with W being the basic hyperelastic strain energy function, λ_i being the principal stretches, and Ω_i being a directional damage parameter, which was cast as a specific sigmoid-type function [27]:

$$\Omega_i = a - \frac{1}{b + \exp\left[-c\left(\lambda_i^{max} - \lambda_i\right)\left(\lambda_i^{max} - 1\right)\right]}\,, \tag{14}$$

where:

$$a\,, b\,, c \in \mathbb{R}^+\,, \tag{15}$$

i.e., are positive real-valued model parameters. It is important to note that in the undeformed configuration there is no damage, i.e., $\Omega_i = 1$, and thus it is required:

$$1 = a - \frac{1}{b+1} \Longrightarrow a = \frac{b+2}{b+1}. \tag{16}$$

Therefore, Ω_i in Eq. (14) has only two parameters; b and c. The total damage parameter Ω is then defined as the average sum of Ω_i as:

$$\Omega = \frac{1}{3}\sum_{i=1} \Omega_i\,, \quad i = 1, 2, 3\,. \tag{17}$$

Thus Ω too has only two parameters; b and c. Finally, the dependence of $\widetilde{W}$ on λ_i and Ω_i was considered to be [27]:

$$\Gamma_i = \Omega_i^{\kappa}\lambda_i\,, \quad i = 1, 2, 3\,, \tag{18}$$

where κ is a real-valued constant; i.e., $\kappa \in \mathbb{R}$, and may be considered as a *modulating* factor in converting the amount of damage into the amount of residual stretch. Hence, $\widetilde{W} = W\left(\Gamma_i\right)$, with $i = 1, 2, 3$.

The foregoing formulations were presented in [27] on using the principal stretches λ_i, since the basic hyperelastic function used therein was the non-separable principal stretches-based *comprehensive* model of [40]. Here, instead, we wish to utilise the principal invariants-based model of Eq. (1), and thus the foregoing derivations need to be reformulated in terms of the principal invariants. Accordingly, on using the definition of Γ_i in Eq. (18), we define the pseudo-invariants $\tilde{I}_i$ as:

$$\begin{cases} \tilde{I}_1 = \Gamma_1^2 + \Gamma_2^2 + \Gamma_3^2 = \Omega_1^{2\kappa}\lambda_1^2 + \Omega_2^{2\kappa}\lambda_2^2 + \Omega_3^{2\kappa}\lambda_3^2 , \\ \tilde{I}_2 = \Gamma_1^{-2} + \Gamma_2^{-2} + \Gamma_3^{-2} = \Omega_1^{-2\kappa}\lambda_1^{-2} + \Omega_2^{-2\kappa}\lambda_2^{-2} + \Omega_3^{-2\kappa}\lambda_3^{-2} . \end{cases} \tag{19}$$

It follows that:

$$\frac{\partial \tilde{I}_1}{\partial \Gamma_i} = 2\Gamma_i , \quad \frac{\partial \tilde{I}_2}{\partial \Gamma_i} = -2\Gamma_i^{-3} . \tag{20}$$

Using the chain rule, the representation formula for the Cauchy stress in Eq. (12) may be rewritten as:

$$T_i = \Omega \left[2\Gamma_i^2 \frac{\partial \widetilde{W}}{\partial \tilde{I}_1} - 2\Gamma_i^{-2} \frac{\partial \widetilde{W}}{\partial \tilde{I}_2} \right] - p , \quad i = 1, 2, 3, \tag{21}$$

where now $\widetilde{W} \equiv W(I_i, \Omega_i) = W(\tilde{I}_i)$:

$$\begin{aligned} \widetilde{W} &= W(\tilde{I}_i) \\ &= \sum_{j=1} \frac{3(n_j - 1)}{2n_j} \mu_j N_j \left[\frac{1}{3N_j(n_j-1)} \left(\tilde{I}_1 - 3\right)^{\beta_j} - \ln\left(\frac{\tilde{I}_1 - 3N_j}{3 - 3N_j}\right)^{\beta_j} \right] \\ &+ \sum_{k=1} C_k \left[\left(\frac{\tilde{I}_2}{3}\right)^{\epsilon_k} - 1 \right] . \end{aligned} \tag{22}$$

Under uniaxial tension where we have $\lambda_1 = \lambda \geq 1$ and $\lambda_2 = \lambda_3 = \lambda^{-0.5} \leq 1$, it is clear from the definition of Ω_i in Eq. (14) that $\Omega_2 = \Omega_3 = 1$, since $\lambda_2^{max} = \lambda_3^{max} = 1$. Therefore, from Eq. (19) we get that: $\tilde{I}_1 = \Omega_1^{2\kappa}\lambda^2 + 2\lambda^{-1}$ and $\tilde{I}_2 = \Omega_1^{-2\kappa}\lambda^{-2} + 2\lambda$. On the assumption of plane stress ($T_{33} = 0$), we find from Eq. (21):

$$T_i = \Omega \left[2\frac{\partial \widetilde{W}}{\partial \tilde{I}_1}\left(\Gamma_i^2 - \Gamma_3^2\right) - 2\frac{\partial \widetilde{W}}{\partial \tilde{I}_2}\left(\Gamma_3^{-2} - \Gamma_i^{-2}\right) \right] , \quad i = 1, 2, 3, \tag{23}$$

which leads to the following explicit Cauchy stress – deformation relationship:

$$\begin{aligned} T_{uni} = \Omega \Bigg\{ \sum_{j=1} \frac{\mu_j \beta_j}{n_j} & \frac{\tilde{I}_1 \left(\tilde{I}_1 - 3\right)^{\beta_j - 1} + 3N_j \left[1 - \left(\tilde{I}_1 - 3\right)^{\beta_j - 1}\right] - 3n_j N_j}{\tilde{I}_1 - 3N_j} \\ & \times \left(\Omega_1^{2\kappa}\lambda^2 - \frac{1}{\lambda}\right) + \sum_{k=1} \frac{2C_k \epsilon_k}{3^{\epsilon_k}} \tilde{I}_2^{\epsilon_k - 1} \left(\lambda - \frac{1}{\Omega_1^{2\kappa}\lambda^2}\right) \Bigg\} , \end{aligned} \tag{24}$$

Table 5 Model parameter values for the discontinuous softening behaviour of nematic-genesis polydomain LCE samples due to Merkel et al. [11], tested at 39 °C, using the one-term expansion of the model. Note that $R^2_{\text{loading}} = 0.99_9$ and $R^2_{\text{unloading}} = 0.99_8$, for the loading and unloading paths, respectively

μ [kPa]	N [-]	n [-]	β [-]	C_2 [kPa]	ϵ [-]	b [-]	c [-]	κ [-]
31.99	0.98	0.95	1.86	311.51	0.50	0.03	1.57	0.001

or equivalently,

$$P_{uni} = \Omega \left\{ \sum_{j=1} \frac{\mu_j \beta_j}{n_j} \frac{\tilde{I}_1 \left(\tilde{I}_1 - 3\right)^{\beta_j - 1} + 3N_j \left[1 - \left(\tilde{I}_1 - 3\right)^{\beta_j - 1}\right] - 3n_j N_j}{\tilde{I}_1 - 3N_j} \right.$$
$$\left. \times \left(\Omega_1^{2\kappa} \lambda - \frac{1}{\lambda^2}\right) + \sum_{k=1} \frac{2C_k \epsilon_k}{3^{\epsilon_k}} \tilde{I}_2^{\epsilon_k - 1} \left(1 - \frac{1}{\Omega_1^{2\kappa} \lambda^3}\right) \right\}, \tag{25}$$

in terms of the engineering stress.

The relationship in Eq. (25), upon using the one-term expansion, is now fitted to the uniaxial loading – unloading data of Merkel et al. [11], tested at 39 °C. The numerical datapoints pertaining to this dataset have been tabulated in Appendix A, Table 11. The fitting results are given in Fig. 6, and the obtained model parameter values are listed in Table 5. With a total of nine model parameters, i.e., μ, N, n, β, C_2 and ϵ of the basic hyperelastic function and b, c and κ for the pseudo-elastic behaviour, it is observed that the model captures the softening in the unloading path, as well as the permanent set, most favourably. The R^2 values are in excess of 0.99. The model also captures the reported stress – deformation data for tests carried out at 19 °C, 62 °C and 89 °C in [11], with different model parameter values. However, we refrain from replicating those results here, as they would only serve to repeat the modelling results already showcased on using the data obtained at 39 °C. We note here that temperature-dependency has not been considered and incorporated into our model. One way of incorporating the temperature effects may be to consider the model parameters to *evolve* with temperature; i.e., are a function of the temperature. A similar approach in relation to incorporating the rate-effects has been devised and presented in [41], using the model in [40] as the basic hyperelastic function.

4.4 The Uniaxial Behaviour of a Monodomain LCE Sample with Auxetic Behaviour

Auxetic behaviour in a specimen under deformation broadly refers to the expansion of that specimen in at least one direction orthogonal to that along which it is being deformed. In a classical incompressible material under uniaxial extension, say along λ_1, one would have that: $\lambda_2 = \lambda_3 = \lambda_1^{-0.5}$. However, in an auxetic incompressible solid, this relationship no longer holds true, as at least one of the either λ_2 or λ_3 are expected to increase.

In a recent study by Raistrick et al. [10], they reported observations on the auxetic behaviour of their acrylate-based monodomain LCE specimens under uniaxial tension, where the overall volume was preserved but the sample dimension increased in one direction, namely the thickness (say λ_3), beyond a threshold applied stretch. Before that threshold

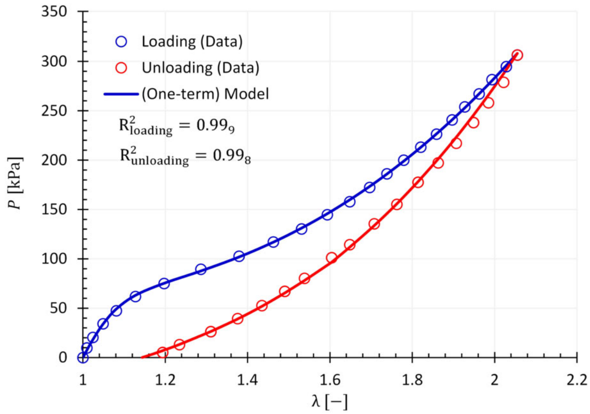

Fig. 6 Modelling results for the uniaxial loading – unloading of a nematic-genesis polydomain LCE sample due to Merkel et al. [11], tested at 39 °C. See the on-line version for plots in colour

stretch is reached, the samples exhibited the classical behaviour; i.e., no auxetics. See the plot in Fig. 7(c).

Based on their observation and results, Mihai et al. [23] developed a mathematical model which was able to capture the uniaxial deformation of the said auxetic specimens. Therein they use an Ogden-type function to describe the strain energy of the deformation, within a framework augmented by the usual 'spontaneous deformation' tensor and the director orientation etc, with a total of nine identifiable model parameters. We also note the application of the Ogden model [42] to capturing auxetic behaviour in other soft solids such as polyurethane foams (e.g., [43]).

Here, using the reported values of λ_3 (i.e., deformation along the thickness) and the uniaxial deformation data in [10], we model the said deformation behaviour with the one-term expansion of the hyperelastic strain energy function in Eq. (1). We emphasise that monodomain LCEs possess anisotropic mechanical properties, and thus their deformation behaviour may not be simulated using an isotropic model. However, to the extent that only the uniaxial mechanical behaviour/deformation is considered, and to merely showcase the capability of our model to capture the auxetic behaviour, we proceed here with such modelling application. For capturing the full anisotropic behaviour, our proposed model may be considered as the basic hyperelastic function to incorporate the preferred direction(s) and anisotropy etc.

In this spirit, for modelling this dataset we first note that $\lambda_1\lambda_2\lambda_3 = 1$ due to incompressibility. Accordingly, from the reported corresponding pair of λ_1 and λ_3 values in the data at each point of deformation, the value of λ_2 is determined, and we note that $I_1 = \lambda_1^2 + \lambda_2^2 + \lambda_3^2$ and $I_2 = \lambda_1^{-2} + \lambda_2^{-2} + \lambda_3^{-2}$. The ensuing $T_{uni} - \lambda_1$ relationship now is:

$$T_{uni} = \frac{\mu\beta}{n} \frac{I_1 (I_1 - 3)^{\beta-1} + 3N \left[1 - (I_1 - 3)^{\beta-1}\right] - 3nN}{I_1 - 3N} \left(\lambda_1^2 - \lambda_3^2\right) + \frac{2C_2\,\epsilon}{3^\epsilon} I_2^{\epsilon-1} \left(\frac{1}{\lambda_3^2} - \frac{1}{\lambda_1^2}\right), \tag{26}$$

Table 6 Obtained model parameter values for the auxetic behaviour of monodomain LCE specimens due to Raistrick et al. [10] using the one-term expansion of the model. Note that $R^2 = 0.99_9$

μ [MPa]	N [-]	n [-]	β [-]	C_2 [MPa]	ϵ [-]
0.17	48.70	8.57_5	3.07	3.26	0.41

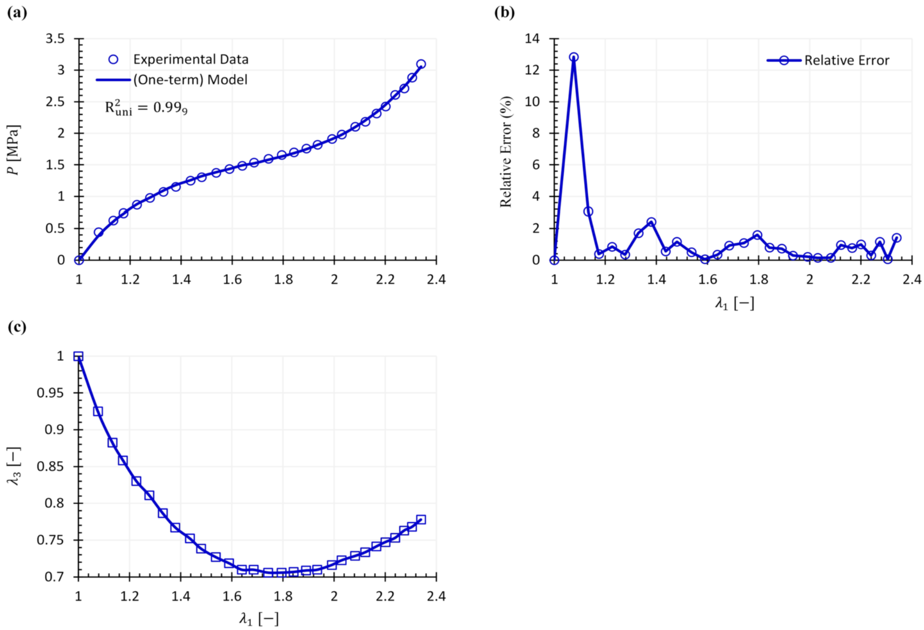

Fig. 7 Modelling the auxetic behaviour of monodomain LCE specimens due to Raistrick et al. [10] using the one-term expansion of the model: (a) fitting to the uniaxial deformation data; (b) the ensuing relative error; and (c) the measured variation of λ_3 versus the λ_1, indicative of the auxetic behaviour

which renders:

$$
\begin{aligned}
P_{uni} = & \frac{\mu\beta}{n} \frac{I_1 (I_1 - 3)^{\beta-1} + 3N \left[1 - (I_1 - 3)^{\beta-1}\right] - 3nN}{I_1 - 3N} \left(\lambda_1 - \frac{\lambda_3^2}{\lambda_1}\right) \\
& + \frac{2C_2 \epsilon}{3^\epsilon} I_2^{\epsilon-1} \left(\frac{1}{\lambda_1 \lambda_3^2} - \frac{1}{\lambda_1^3}\right),
\end{aligned}
\tag{27}
$$

in terms of the engineering stress.

Equation (27) was fitted to the data from [10], and the modelling results are shown the plots in Fig. 7. The identified model parameter values have been summarised in Table 6. The tabulated numerical datapoints collated from [10] have been presented in Table 12 of Appendix A. The favourability of the results is apparent, with R^2 values in excess of 0.99. Comparing the modelling results with that of [23], Fig. 4 therein, the improvement provided by the model here is encouraging. This improvement is further reflected in the relative error plot of Fig. 7(b), compared with that of Fig. 4 in [23].

5 Concluding Remarks

Single- and multi-mode deformations of polydomain LCEs, including isotropic- and nematic-genesis, and encompassing uniaxial and pure shear deformations, were modelled in this work on using a hyperelastic strain energy function, presented in Eq. (1). The modelling approach here departed from the neo-classical theory of liquid crystal elastomers, and only utilised a strain energy function W. Complex phenomena such as the soft elasticity behaviour were therefore captured and modelled as a state of hyperelasticity, without incorporating a 'step-length' tensor or the 'anisotropy parameter' which are typical of neo-classical LCE models. The considered model here was shown to capture the deformation of the samples most favourably, on using one-, two-, or three-term expansions.

The model was then applied to capturing additional features such as the continuous (i.e., in the primary loading path) and discontinuous (i.e., in the unloading path) softening, as well as the auxetic, behaviours of LCE samples. Except for the discontinuous softening behaviour, where the addition of a usual scalar damage parameter was required, the considered behaviours were captured and modelled by the basic hyperelastic model (1), without the need for further augmentation or extra model parameters. Features such as softening in the unloading path and the permenant set were also captured by using minimal number of model parameters; e.g., only the one-term expansion of the model and a single damage parameter. The correlation between the model predictions and the experimental data was shown to be of a close affinity.

The presented modelling results in this work appear to suggest that many complex mechanical features of (polydomain) LCEs may be regarded as (new) states of hyperelasticity, capturable by an appropriate form of hyperplastic strain energy function. The W function in Eq. (1) appears to be a suitable model in this regard. A hyperelastic modelling approach to the deformation of LCEs would simplify the modelling efforts considerably, by doing away with the complexities that arise as a result of incorporating a 'step-length' tensor or the 'anisotropy parameter', as well as ameliorating the shortcomings of the neo-classical theory as outlined in §1. Given the success of the current model in this study, further exploration of the application of this modelling approach to multiaxial deformation of LCEs and other deformation modes such as inflation etc may be merited. Furthermore, in applications where features such as anisotropy, rate- and/or temperature dependence, or more complex phenomena are involved, the presented model here may be considered as a hyperplastic backbone in the neo-classical theory or other modelling frameworks for more accurate modelling results.

Appendix A: Tabulated Numerical Datapoints of the Datasets Used in This Work

Table 7 Data for the multimodal deforamtions carried out on our nematic-genesis polydomain LCE samples

Uniaxial Deformation		Pure Shear Deformation	
λ [-]	P_{uni} [MPa]	λ [-]	P_{ps} [MPa]
1	0	1	0
1.05	0.12	1.02	0.04
1.10	0.21	1.03	0.07
1.15	0.28	1.04	0.09
1.20	0.32_5	1.05	0.11
1.30	0.37	1.07	0.16
1.40	0.39	1.08	0.18
1.50	0.40	1.09	0.21
1.55	0.41	1.10	0.23
1.60	0.43	1.11	0.25
1.70	0.46	1.12_5	0.27
1.75	0.48	1.14	0.29
1.80	0.50_5	1.15_5	0.32
1.85	0.53	1.17	0.34
1.90	0.56	1.18_5	0.36
2.00	0.63	1.20	0.37
2.10	0.70	1.21_5	0.39
2.15	0.74	1.22_5	0.41
2.20	0.79	1.24	0.42
2.25	0.84	1.26	0.45
2.30	0.89	1.27_5	0.46
2.35	0.95_5	1.30	0.48
2.40	1.02	1.32	0.50
2.45	1.10	1.34	0.51_5
2.50	1.18	1.36	0.53
2.55	1.27	1.37_5	0.54
2.60	1.37	1.40	0.55
2.65	1.47	1.42	0.56
2.70	1.59	1.44	0.57_5
2.75	1.71	1.46	0.59
2.85	2.00	1.48	0.60
2.90	2.15	1.50	0.61

Table 8 Data for the multimodal deforamtions carried out on our isotropic-genesis polydomain LCE specimens

Uniaxial Deformation		Pure Shear Deformation	
λ [-]	P_{uni} [MPa]	λ [-]	P_{ps} [MPa]
1	0	1	0
1.15	0.03	1.05	0.01
1.27_5	0.05_1	1.10	0.01_6
1.40	0.05_2	1.15	0.02_1
1.60	0.05_3	1.20	0.02_5
1.75	0.05_4	1.25	0.02_9
1.90	0.058	1.30	0.03
2.00	0.06	1.40	0.03_5
2.21	0.07	1.50	0.04
2.51	0.09	1.60	0.04_3
2.81	0.10_5	1.70	0.05
3.11	0.11	1.75	0.05_2
3.41	0.13_5	1.80	0.06
3.55	0.14_5	1.90	0.06_4
3.72	0.16	2.00	0.07
4.02	0.18	2.05	0.07_5
4.20	0.20	2.10	0.08
4.32	0.21	2.20	0.08_7
4.62	0.26	2.30	0.09
4.92	0.29	2.40	0.10
5.23	0.34	2.50	0.11
5.53	0.40	2.60	0.11_5
5.83	0.49	2.70	0.12
5.95	0.54	2.80	0.13
6.13	0.61	2.90	0.13_5
6.30	0.70	3.00	0.14
6.43	0.79	3.01	0.14_2

Table 9 Datapoints of the uniaxial and pure shear deformation tests due to Tokumoto et al. [4] on their isotropic-genesis polydomain specimens

Uniaxial Deformation		Pure Shear Deformation	
λ [-]	T_{uni} [kPa]	λ [-]	T_{ps} [kPa]
1	0	1	0
1.20	17.78	1.20	22.35
1.40_5	21.48	1.40	31.77
1.59_5	22.22	1.60	40.00
1.80	22.96	1.80	51.77
2.00	26.67	2.00	63.53
2.19	35.55_5	2.20	74.12
2.39	54.81_5	2.40	85.88
2.58	85.93	2.60	97.65
2.78	115.55_5	2.80	111.77
2.99	142.22	3.00	129.41
3.18	171.85	3.20	148.23_5
3.38	201.48	3.40	168.23_5
3.58	232.59	3.60	190.59
3.78	266.67	3.80	214.12

Table 10 Datapoints of the nematic LCE samples due to He et al. [25] under uniaxial deformation

λ [-]	P [MPa]
1	0
1.19	0.001
1.36	0.002
1.58	0.003
1.83	0.004
1.98	0.006
2.16	0.02
2.27	0.04
2.39	0.07
2.46	0.09
2.56	0.12
2.65	0.15
2.81	0.20
2.96	0.24
3.07	0.27
3.19	0.30

Table 11 Datapoints of the uniaxial loading/unloading tests performed on nematic-genesis polydomain LCE samples due to Merkel et al. [11], tested at 39 °C

Loading		Unloading	
λ [-]	P [kPa]	λ [-]	P [kPa]
1	0	2.05_5	306.58
1.01	9.87	2.02	278.95
1.02	20.39_5	1.98_5	258.21
1.05	34.21	1.95	238.16
1.08	47.37	1.91	217.10_5
1.13	61.84	1.86	197.37
1.20	75.00	1.81	177.63
1.29	89.47	1.76	155.26
1.38	102.63	1.71	135.53
1.46	117.10_5	1.65	114.47
1.53	130.26	1.60	101.32
1.59	144.74	1.54	80.26
1.65	157.89_5	1.49	67.10_5
1.70	172.37	1.43_5	52.63
1.74	186.18	1.38	39.47
1.78	200.00	1.31	26.32
1.82	213.16	1.23_5	13.16
1.86	226.32	1.19	5.26
1.90	240.79		
1.93	253.95		
1.96	267.10_5		
1.99	281.58		
2.03	294.74		
2.05_5	306.58		

Table 12 Numerical data for the monodomain LCE specimen due to Raistrick et al. [10] exhibiting auxetic behaviour under uniaxial deformation

λ_1 [-]	P [MPa]	λ_3 [-]
1	0	1
1.08	0.44_5	0.92_5
1.13	0.63	0.88
1.17_5	0.74	0.86
1.23	0.87	0.83
1.28	0.98	0.81
1.33	1.07	0.79
1.38	1.15	0.77
1.44	1.25	0.75
1.48	1.30_5	0.74
1.54	1.38	0.73
1.59	1.44	0.72
1.64	1.49	0.71
1.68_5	1.54	0.71
1.74	1.60	0.71
1.79	1.66	0.71
1.84	1.70	0.71
1.89	1.76	0.71
1.93	1.82	0.71
1.99	1.91	0.72
2.03	1.98	0.72
2.08	2.10	0.73
2.12	2.18_5	0.73
2.16_5	2.32	0.74
2.20	2.43	0.75
2.24	2.61	0.75
2.27_5	2.71	0.76
2.30_5	2.88	0.77
2.34	3.10	0.78

Appendix B: Further Modelling Results to Those Presented in the Main Text on Using the Proposed Model

Table 13 Obtained model parameter values identified by fitting the one-term expansion of the model to the mutimodal deformation dataset in the plots of Fig. 8, of our nematic-genesis polydomain LCE specimen. Note that $R^2_{uni} = 0.99_6$ and $R^2_{ps} = 0.99_1$, for uniaxial and pure shear deformations, respectively

μ [MPa]	N [-]	n [-]	β [-]	C_2 [MPa]	ϵ [-]
0.02_5	0.93	0.65	2.16	2.83	0.28

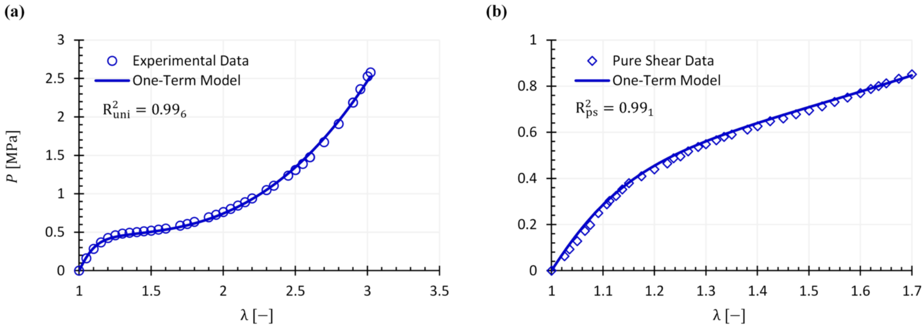

Fig. 8 An additional modelling result for uniaxial and pure shear deformations from our in-house nematic-genesis polydomain LCE specimens using the one-term expansion of the model in Eq. (1): (a) uniaxial; and (b) pure shear deformations

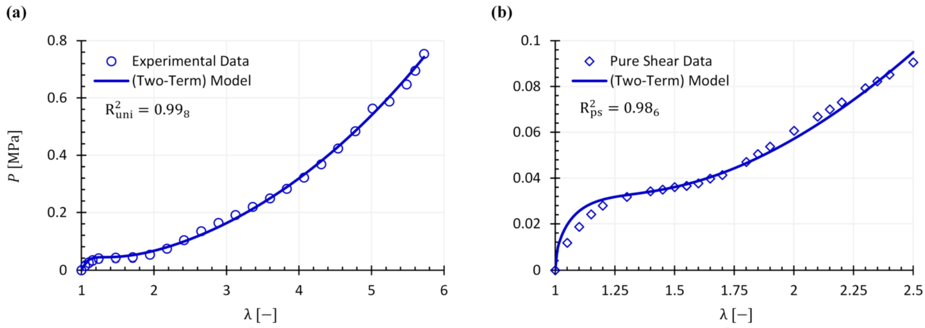

Fig. 9 An additional modelling result for uniaxial and pure shear deformations from our in-house isotropic-genesis polydomain LCE specimens using the two-term expansion of the model in Eq. (1): (a) uniaxial; and (b) pure shear deformations

Table 14 The identified model parameter values using the dataset in the plots of Fig. 9, from our isotropic-genesis polydomain samples. Note that $R^2_{uni} = 0.99_8$ and $R^2_{ps} = 0.98_6$, for uniaxial and pure shear deformations, respectively

μ_1 [MPa]	N_1 [-]	n_1 [-]	β_1 [-]	C_1 [MPa]	ϵ_1 [-]
0.00_3	0.89_5	0.78	1.80	3.88	0.15
μ_2 [MPa]	N_2 [-]	n_2 [-]	β_2 [-]	C_2 [MPa]	ϵ_2 [-]
0.05	0.00_4	0.90	0.79	-3.73	0.17

Fig. 10 Modelling results for the nematic LCE specimens of He et al. [25] under uniaxial deformation on using the one-term expansion of the model

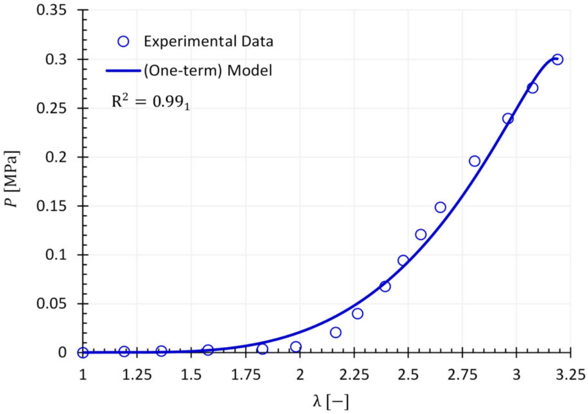

Table 15 Model parameter values for the nematic LCE specimens of He et al. [25] under uniaxial deformation on using the one-term expansion of the model. Note that $R^2 = 0.99_1$

μ [MPa]	N [-]	n [-]	β [-]	C_2 [MPa]	ϵ [-]
0.001	3.87_5	0.55	2.60	6.35	0.0009

Acknowledgements Z.W. and R.B. are grateful for the support of the National Science Foundation (USA) through grant CMMI-2146409.

Author contributions A.A. and R.B. designed the research. A.A. performed the theoretical modelling. Z.W. performed the experiment. A.A. wrote the first draft of the paper. All authors contributed to the writing of the final manuscript.

Funding Open access funding provided by Northeastern University Library.

Data Availability Data is provided within the manuscript or appendix.

Declarations

Competing interests The authors declare no competing interests.

References

1. Traugutt, N.A., Volpe, R.H., Bollinger, M.S., Saed, M.O., Torbati, A.H., Yu, K., Dadivanyan, N., Yakacki, C.M.: Liquid-crystal order during synthesis affects main-chain liquid-crystal elastomer behaviour. Soft Matter **13**, 7013–7025 (2017). https://doi.org/10.1039/C7SM01405H

2. Biggins, J.S., Warner, M., Bhattacharya, K.: Elasticity of polydomain liquid crystal elastomers. J. Mech. Phys. Solids **60**, 573–590 (2012). https://doi.org/10.1016/j.jmps.2012.01.008
3. Wei, Z., Wang, P., Bai, R.: Thermomechanical coupling in polydomain liquid crystal elastomers. J. Appl. Mech. **91**, 021001 (2024). https://doi.org/10.1115/1.4063219
4. Tokumoto, H., Zhou, H., Takebe, A., Kamitani, K., Kojio, K., Takahara, A., Bhattacharya, K., Urayama, K.: Probing the in-plane liquid-like behavior of liquid crystal elastomers. Sci. Adv. **7**, eabe9495 (2021). https://doi.org/10.1126/sciadv.abe9495
5. Lee, V., Bhattacharya, K.: Universal deformations of incompressible nonlinear elasticity as applied to ideal liquid crystal elastomers. J. Elast. (2023). https://doi.org/10.1007/s10659-023-10018-9
6. Urayama, K., Kohmon, E., Kojima, M., Takigawa, T.: Polydomain – monodomain transition of randomly disordered nematic elastomers with different cross-linking histories. Macromolecules **42**, 4084–4089 (2009). https://doi.org/10.1021/ma9004692
7. Biggins, J.S., Warner, M., Bhattacharya, K.: Supersoft elasticity in polydomain nematic elastomers. Phys. Rev. Lett. **103**, 037802 (2010). https://doi.org/10.1103/PhysRevLett.103.037802
8. Mistry, D., Morgan, P.B., Clamp, J.H., Gleeson, H.F.: New insights into the nature of semi-soft elasticity and "mechanical-Fréedericksz transitions" in liquid crystal elastomers. Soft Matter **14**, 1301–1310 (2018). https://doi.org/10.1039/C7SM02107K
9. Mistry, D., Connel, S.D., Mickthwaite, S.L., Morgan, P.B., Clamp, J.H., Gleeson, H.F.: Coincident molecular auxeticity and negative order parameter in a liquid crystal elastomer. Nat. Commun. **9**, 5095 (2018). https://doi.org/10.1038/s41467-018-07587-y
10. Raistrick, T., Zhang, Z., Mistry, D., Mattsson, J., Gleeson, H.F.: Understanding the physics of the auxetic response in a liquid crystal elastomer. Phys. Rev. Res. **3**, 023191 (2021). https://doi.org/10.1103/PhysRevResearch.3.023191
11. Merkel, D.R., Shaha, R.K., Yakacki, C.M., Frick, C.P.: Mechanical energy dissipation in polydomain nematic liquid crystal elastomers in response to oscillating loads. Polymer **166**, 148–154 (2019). https://doi.org/10.1016/j.polymer.2019.01.042
12. Warner, M., Gelling, K.P., Vilgis, T.A.: Theory of nematic networks. J. Chem. Phys. **88**, 4008–4013 (1988). https://doi.org/10.1063/1.453852
13. Warner, M., Wang, X.J.: Elasticity and phase behavior of nematic elastomers. Macromolecules **24**, 4932–4941 (1991). https://doi.org/10.1021/ma00017a033
14. Bladon, P., Terentjev, E.M., Warner, M.: Transitions and instabilities in liquid crystal elastomers. Phys. Rev. E **47**, R3838–R3840 (1993). https://doi.org/10.1103/PhysRevE.47.R3838
15. Bladon, P., Terentjev, E.M., Warner, M.: Deformation-induced orientational transitions in liquid crystal elastomers. J. Phys. II **4**, 75–91 (1994). https://doi.org/10.1051/jp2:1994100
16. DeSimone, A., Teresi, L.: Elastic energies for nematic elastomers. Eur. Phys. J. E **29**, 191–204 (2009). https://doi.org/10.1140/epje/i2009-10467-9
17. Agostiniani, V., DeSimonel, A.: Ogden-type energies for nematic elastomers. Int. J. Non-Linear Mech. **47**, 402–412 (2012). https://doi.org/10.1016/j.ijnonlinmec.2011.10.001
18. Anssari-Benam, A., Horgan, C.O.: On modelling simple shear for isotropic incompressible rubber-like materials. J. Elast. **147**, 83–111 (2021). https://doi.org/10.1007/s10659-021-09869-x
19. Anssari-Benam, A., Destrade, M., Saccomandi, G.: Modelling brain tissue elasticity with the Ogden model and an alternative family of constitutive models. Philos. Trans. R. Soc. Lond. Ser. A **380**, 20210325 (2022). https://doi.org/10.1098/rsta.2021.0325
20. Anssari-Benam, A.: Comparative modelling results between a separable and a non-separable form of principal stretches–based strain energy functions for a variety of isotropic incompressible soft solids: Ogden model compared with a parent model. Mech. Soft Mater. **5**, 2 (2023). https://doi.org/10.1007/s42558-023-00050-z
21. Fried, E., Sellers, S.: Soft elasticity is not necessary for striping in nematic elastomers. J. Appl. Phys. **100**, 043521 (2006). https://doi.org/10.1063/1.2234824
22. Mihai, L.A., Goriely, A.: A pseudo-anelastic model for stress softening in liquid crystal elastomers. Proc. R. Soc. A **476**, 20200558 (2020). https://doi.org/10.1098/rspa.2020.0558
23. Mihai, L.A., Mistry, D., Raistrick, T., Gleeson, H.F., Goriely, A.: A mathematical model for the auxetic response of liquid crystal elastomers. Philos. Trans. R. Soc. Lond. Ser. A **380**, 20210326 (2022). https://doi.org/10.1098/rsta.2021.0326
24. Anssari-Benam, A.: Continuous softening up to the onset of failure: a hyperelastic modelling approach with intrinsic softening for isotropic incompressible soft solids. Mech. Res. Commun. **132**, 104183 (2023). https://doi.org/10.1016/j.mechrescom.2023.104183
25. He, Q., Zheng, Y., Wang, Z., He, X., Cai, S.: Anomalous inflation of a nematic balloon. J. Mech. Phys. Solids **142**, 104013 (2020). https://doi.org/10.1016/j.jmps.2020.104013
26. Ogden, R.W., Roxburgh, D.G.: A pseudo–elastic model for the Mullins effect in filled rubbe. Proc. R. Soc. Lond. A **455**, 2861–2877 (1999). https://doi.org/10.1098/rspa.1999.0431

27. Anssari-Benam, A., Akbari, R., Dargazany, R.: Extending the theory of pseudo-elasticity to capture the permanent set and the induced anisotropy in the Mullins effect. Int. J. Non-Linear Mech. **156**, 104500 (2023). https://doi.org/10.1016/j.ijnonlinmec.2023.104500
28. Anssari-Benam, A.: A generalised $W(I_1, I_2)$ strain energy function of binomial form with unified applicability across various isotropic incompressible soft solids. Acta Mech. **235**, 99–132 (2024). https://doi.org/10.1007/s00707-023-03677-1
29. Anssari-Benam, A.: On a new class of non-Gaussian molecular based constitutive models with limiting chain extensibility for incompressible rubber-like materials. Math. Mech. Solids **26**, 1660–1674 (2021). https://doi.org/10.1177/10812865211001094
30. Carroll, M.M.: A strain energy function for vulcanized rubbers. J. Elast. **103**, 173–187 (2011). https://doi.org/10.1007/s10659-010-9279-0
31. Mihai, L.A., Goriely, A.: Positive or negative Poynting effect? The role of adscititious inequalities in hyperelastic materials. Proc. R. Soc. Lond. A **467**, 3633–3646 (2011). https://doi.org/10.1098/rspa.2011.0281
32. Treloar, L.R.G.: The elasticity of a network of long-chain molecules - II. Trans. Faraday Soc. **39**, 241–246 (1943). https://doi.org/10.1039/TF9433900241
33. Gent, A.N.: A new constitutive relation for rubber. Rubber Chem. Technol. **69**, 59–61 (1996). https://doi.org/10.5254/1.3538357
34. Anssari-Benam, A., Horgan, C.O.: A three-parameter structurally motivated robust constitutive model for isotropic incompressible unfilled and filled rubber-like materials. Eur. J. Mech. A, Solids **95**, 104605 (2022). https://doi.org/10.1016/j.euromechsol.2022.104605
35. Anssari-Benam, A., Bucchi, A.: Modelling the deformation of the elastin network in the aortic valve. J. Biomech. Eng. **140**, 011004 (2018). https://doi.org/10.1115/1.4037916
36. Anssari-Benam, A., Bucchi, A.: A generalised neo-Hookean strain energy function for application to the finite deformation of elastomers. Int. J. Non-Linear Mech. **128**, 103626 (2021). https://doi.org/10.1016/j.ijnonlinmec.2020.103626
37. Saed, M.O., Torbati, A.H., Nair, D.P., Yakacki, C.M.: Synthesis of programmable main-chain liquid-crystalline elastomers using a two-stage thiol-acrylate reaction. J. Vis. Exp. **107**, 53546 (2016). https://doi.org/10.3791/53546
38. Traugutt, N.A., Volpe, R.H., Bollinger, M.S., Saed, M.O., Torbati, A.H., Yu, K., Dadivanyanc, N., Yakacki, C.M.: Liquid-crystal order during synthesis affects main-chain liquid-crystal elastomer behavior. Soft Matter **13**, 7013–7025 (2017). https://doi.org/10.1039/C7SM01405H
39. Dorfmann, A., Ogden, R.W.: A constitutive model for the Mullins effect with permanent set in particle-reinforced rubber. Int. J. Solids Struct. **41**, 1855–1878 (2004). https://doi.org/10.1016/j.ijsolstr.2003.11.014
40. Anssari-Benam, A.: Large isotropic elastic deformations: on a comprehensive model to correlate the theory and experiments for incompressible rubber-like materials. J. Elast. **153**, 219–244 (2023). https://doi.org/10.1007/s10659-022-09982-5
41. Anssari-Benam, A., Hossain, M.: A pseudo-hyperelastic model incorporating the rate effects for isotropic rubber-like materials. J. Mech. Phys. Solids **179**, 105347 (2023). https://doi.org/10.1016/j.jmps.2023.105347
42. Ogden, R.W.: Large deformation isotropic elasticity – on the correlation of theory and experiment for incompressible rubberlike solids. Proc. R. Soc. Lond. A **326**, 565–584 (1972). https://doi.org/10.1098/rspa.1972.0026
43. Ciambella, J., Bezazi, A., Saccomandi, G., Scarpa, F.: Nonlinear elasticity of auxetic open cell foams modeled as continuum solids. J. Appl. Phys. **117**, 184902 (2015). https://doi.org/10.1063/1.4921101